Progress in Nuclear Energy 163 (2023) 104807

Contents lists available at ScienceDirect

Progress in Nuclear Energy

journal homepage: www.elsevier.com/locate/pnucene

Irradiation and temperature service stability of the radioisotope thermophotovoltaic generators based general purpose heat source

Hongyu Wang [a], Zhiheng Xu [a,b,**], Yunpeng Liu [a,b], Caifeng Meng [a], Xiaobin Tang [a,b,*]

[a] Department of Nuclear Science and Technology, Nanjing University of Aeronautics and Astronautics, Nanjing, 211106, China
[b] Key Laboratory of Nuclear Technology Application and Radiation Protection in Astronautics, Ministry of Industry and Information Technology, Nanjing, 211106, China

ARTICLE INFO

Keywords:
Radioisotope thermophotovoltaic generator
Life evaluation
Neutron/γ irradiation
Radiation damage
Temperature effect

ABSTRACT

Highly stable and long-life power supply systems are crucial to the success of space exploration missions. The systematic analysis of the service lives and stability of radioisotope thermophotovoltaic (RTPV) generators with general purpose heat sources (GPHSs) is the cornerstone of future practical space applications. Its operational lifetime is mainly limited by the degradation caused by the irradiation of key transducer components by the isotope source, while its operational stability is mainly related to the temperature variation of the external environment. The irradiation and temperature stability as the main influencing factors of GPHS-RTPV were studied. Results indicate that the output performance of the GPHS–RTPV was maintained at 50.15% after 1×10^{13} n/cm^2 neutron and 927.84 Gy γ irradiation. The service life was conservatively estimated to be 19.883 years according to equivalent irradiation experimental results. In addition, the output performance of the GPHS–RTPV fluctuates linearly with temperature, the gradient of P_{max} with temperature was −6.7 μW/K·cm^2 in a range of 276.5–354.5 K, and higher output at low temperatures. This study explored the lifetime and service stability of GPHS-RTPV under actual operating conditions in space, and lays the foundation for future practical applications.

1. Introduction

Highly reliable power supply systems are crucial to efficient deep space exploration. Nuclear batteries have long lives and high stability and are unaffected by the external environment, demonstrating their importance as power systems for deep space exploration (Liu et al., 2020a, 2020b; Yuan et al., 2018). In recent years, radioisotope thermophotovoltaic (RTPV) generators, which use radioisotope heat sources to generate electricity, have drawn extensive attention. Given the advantages of high-energy conversion efficiency, specific power, reliability, and simple structure, RTPV generators have become a very promising new-generation space nuclear power sources (Datas and Martí, 2017; H. Wang et al., 2020; X. Wang et al., 2020a). The operating principle of RTPV is the conversion of the thermal energy of decayed radioisotope into electric energy through infrared radiation. An RTPV is mainly composed of radioisotope heat source, emitter, and thermophotovoltaic (TPV) cells. The decay of radioisotopes produces a steady stream of heat, which is transferred to the emitter to generate high temperatures and radiate near-infrared light, and then the TPV cell converts infrared energy into electricity through the photovoltaic effect (Chubb, 2007), as shown in Fig. 1(a).

The stability of RTPV components under actual working conditions is the key to ensuring its overall life and stability. The emitter has excellent irradiation and thermal stability (Wang et al., 2022). The TPV cell is directly involved in photoelectric energy conversion within systems, and it is the most important but the weakest component in RTPV components. Hence, the long-term irradiation and temperature stability of the TPV cell are important factors that directly determine the service lives of the overall RTPV system.

The General-Purpose Heat Source (GPHS) is a mature radioisotope heat source module widely used in many space missions (X. Wang et al., 2020b). The main radioisotope composition of a GPHS is $^{238}PuO_2$, which has a half-life and specific power adapted to RTPV generators. With a decay of ^{238}Pu, a GPHS continuously radiates neutrons and γ rays. The initial total deposition intensity of a 500 W GPHS is approximately 1.492×10^7 neutrons/s and 5.413×10^{13} photons/s (Cheon et al., 2018; Lee et al., 2017), the operating temperature range of surface is usually 887–1211 K (Rinehart, 2001; Vining and Bennett, 2010). The critical components inside the GPHS–RTPV generators are subjected to neutron and γ ray bombardment and high temperature from the GPHS during operation, as shown in Fig. 1(b). In addition, if it orbits the surface of

* Corresponding author. Department of Nuclear Science and Technology, Nanjing University of Aeronautics and Astronautics, Nanjing, 211106, China.
** Corresponding author. Department of Nuclear Science and Technology, Nanjing University of Aeronautics and Astronautics, Nanjing, 211106, China.
E-mail addresses: xuzhiheng@nuaa.edu.cn (Z. Xu), tangxiaobin@nuaa.edu.cn (X. Tang).

https://doi.org/10.1016/j.pnucene.2023.104807
Received 6 August 2022; Received in revised form 26 June 2023; Accepted 5 July 2023
Available online 22 July 2023

Nomenclature

Symbols

T_n	Neutron equivalent service time, yr
T_γ	γ equivalent service time,yr
D_n	Neutron irradiation flux density, n/cm^2
D_{Xd}	Total displacements per atom of XPNR,dpa
D_{Gd}	Displacements per atom per second of GPHS,dpa/s
D_γ	γ irradiation dose, Gy
D_{rn}	Reference neutron flux density, n/s·cm^2
$D_{r\gamma}$	Reference γ dose, Gy/h
R^2	The variance of the fitting curve
C	Fitting parameters
D	Fitting parameters
I	Output current density, μA/cm^2
I_{sc}	Short-circuit current density, μA/cm^2
V	Output voltage, mV
V_{oc}	Open-circuit voltage, mV
P	Power density, μW/cm^2
P_{max}	Maximum output power density, μW/cm^2
FF	Fill factor
Y	Attenuation percentage
E_g	Bandgap, eV
T_c	Temperature of TPV cell, K

Abbreviations

RTPV	Radioisotope Thermophotovoltaic
GPHS	General Purpose Heat Source
InGaAs	Indium Gallium Arsenide
TPV	Thermophotovoltaic
XPNR	Xi'an Pulsed Neutron Reactor
EQE	External Quantum Efficiency
IQE	Internal Quantum Efficiency
DPA	Displacements Per Atom

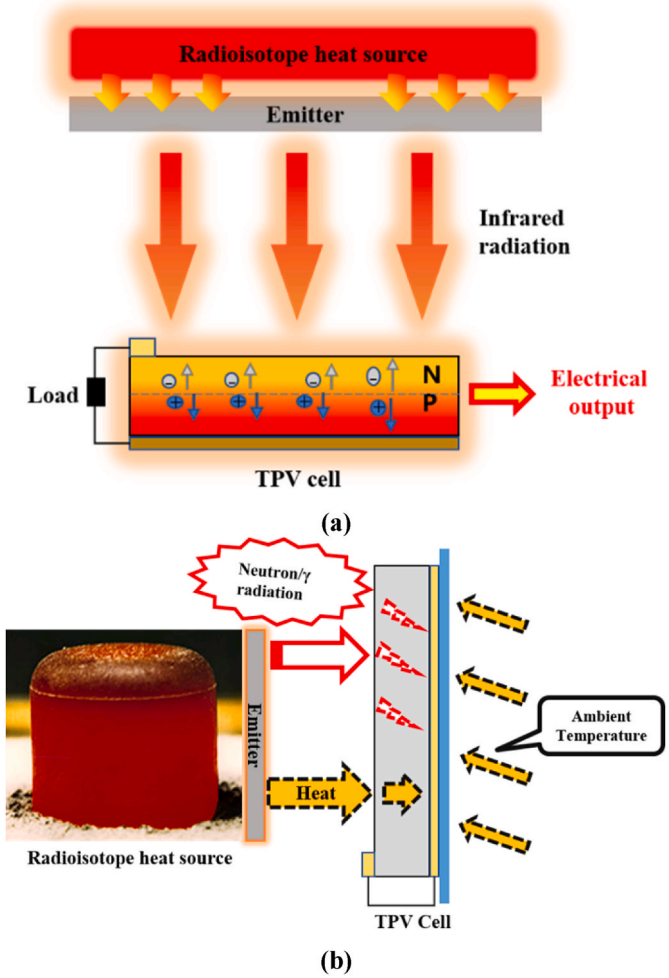

Fig. 1. (a) Schematic of RTPV and (b) schematic of components affected during operation.

Mars, on the one hand there is a certain amount of space radiation, with an average dose of about 9 × 10^{-6} Gy/h due to the protection of the protective shell (Zeitlin et al., 2004). On the other hand, the temperature varies dramatically, and the temperature difference between day and night can even reach 90 K(Liu and Junjun, 2003). The normal operation of GPHS–RTPV generator operating here is maintained by regulating the temperature of the TPV cell through heat-dissipating and thermal management devices, which normally operates within the temperature range of 270–360 K due to the 90 K temperature difference. Alternating ambient temperatures can also have an effect on the system stability of the GPHS–RTPV generators if it is operated in the above mentioned environment.

At present, the research related to RTPV is still in its preliminary stage, the 500W GPHS-RTPV generator (Fig. S1) (Schock et al., 1995, 1996) was proposed and has undergone extensive attention, Crowley (Crowley et al., 2005) and Wolford (Wolford and Chubb, 2009) et al. discussed its structural design and expected performance, both without addressing the lifetime and stability studies of the whole system. For the TPV energy conversion unit, the III–V direct bandgap semiconductor InGaAs TPV cell has attracted considerable interest due to its bandgap tunability and high in-band quantum efficiency (Koudelka et al., 2006; Strauch et al., 2015).The radiation damage caused by multi-junction solar cells for space applications has been extensively investigated (Hongliang et al., 2019; Long et al., 2019). However, reports on the irradiation and temperature effect of a single junction InGaAs cell during infrared energy conversion are few. Martín et al. (Martín and Algora, 2004) and Blandre et al. (2019) analyzed the influence of high temperature on the photoelectric efficiency of GaSb cells through experimentation and simulation, respectively. Nevertheless, InGaAs cells for RTPV and the actual working conditions of GPHS were not discussed. Hence, it is very relevant to study the irradiation and temperature effects of InGaAs cells under actual GPHS conditions to evaluate the lifetime and stability of GPHS-RTPV.

In this work, an RTPV generator with 500 W GPHS was studied, and the relationship between irradiation and temperature variation on their lifetime and operational stability were explored. The InGaAs cell located at the top and bottom of the GPHS-RTPV is a key component to explore its stability and lifetime. Reactor neutron and Co-60 γ sources are used to equate the radiation of GPHS, and the attenuation law of an InGaAs cell under neutron and γ irradiation was studied using the equivalent experiment method. After the equivalent calculation of time epitaxy, the performance degradation characteristics of the InGaAs cell within a specific period of service were evaluated, and its service life was predicted. Using online variable temperature thermophotovoltaic tests, the performance variation patterns of InGaAs cells at different temperatures were investigated. The performance of InGaAs cells showed no fluctuation and degradation under continuous measurements over a continuous period of 300 days, demonstrating excellent stability. This study analyzes the expected lifetime and operational stability of the GPHS-

RTPV generator under actual operating conditions, and also provides a reference and lifetime basis for its future research in practical space applications.

2. Materials and methods

2.1. Experimental conditions and time-equivalent method for accelerated irradiation

$^{238}PuO_2$ decay produces high-energy α particles. However, the range of α particles is very short, only 18 μm in the source core. These α particles are all trapped inside heat sources, and their kinetic energy is converted into the heat energy of a GPHS. In a GPHS, most of the external dose comes from fast neutrons produced by spontaneous fission and (α, n) reactions, and a small part comes from medium- and low-energy γ rays. The neutron intensity produced by spontaneous fission is 2.5×10^3 n/s·g, and the neutrons have an energy range of 0–10 MeV, with an average energy of 2 MeV. The neutron intensity generated by the (α, n) reactions of α particles with ^{18}O and ^{17}O is about 2×10^4 n/s·g, with a maximum energy of 5.8 MeV(Barklay et al., 2005, 2007). Additionally, various decay daughters produced during the decay of radioisotopes generate γ rays during deexcitation. The neutron and γ energy spectra are shown in Fig. S2.

The equivalent accelerated service experimental neutron source for the GPHS was from Xi'an Pulsed Neutron Reactor (XPNR), and the corresponding neutron energy spectrum distribution is shown in Fig. S2 (a). Irradiation at a high temperature may produce annealing effect, affecting the irradiation results. Therefore 300 K was selected as the temperature of irradiation. The range of neutron irradiation dose was broadened by using four cumulative injection values: 4.56×10^{10}, 1×10^{11}, 1×10^{12}, and 1×10^{13} n/cm^2.

For the accelerated irradiation equivalence experiment of γ ray from GPHS, the Co-60 irradiation source in the Radiation Center of Nanjing University of Aeronautics and Astronautics was selected for the equivalent γ irradiation scenario of the RTPV generator. Under a Co-60 γ radiation field with photon energy of 1.25 MeV (50% 1.17 and 50% 1.33 MeV), the dose rate sites of 77.32 Gy/h (Water) were selected. In this experiment, InGaAs cells were irradiated for 4–12 h according to the dose rate calculated using the InGaAs cells in the RTPV generator to meet the matching γ irradiation equivalence.

2.1.1. Neutron radiation dose calculation and equivalence

The heat source of the GPHS–RTPV power supply system was composed of two GPHS modules, and the total thermal power was 500 W. The total neutron intensity was 1.49×10^7 n/s, and the total photon intensity was 5.413×10^{13} p/s. The distance between the InGaAs cell and the heat source center was 10 cm. At a radius of 10 cm, the neutron flux density (D_{rn}) under a unit area of the sphere was 1.1873×10^4 n/s·cm^2.

In the neutron irradiation experiment, the principle of cumulative total particle injection and the total displacements per atom (DPA) were employed to evaluate the equivalent time for neutron irradiation, respectively. The equivalent service time was obtained from the ratio between total cumulative injection and GPHS neutron flux density on the surface of the InGaAs cell by using Formula (1).

$$T_{n1}(yr) = \frac{1}{3600 \times 24 \times 365}(D_n / D_{rn}) \quad (1)$$

where D_n is the total neutron irradiation dose and D_{rn} is the reference neutron flux density.

Equation (2) was employed to calculate the equivalent service time for the total DPA assessment. This method provided an additional level of accuracy, as it took into account the total displacements per atom caused by the neutron exposure.

Table 1
Equivalent calculated values of neutron irradiation.

Properties	Dose point 1	Dose point 2	Dose point 3	Dose point 4
Total irradiation dose density D_n (n/cm^2)	4.56×10^{10}	1×10^{11}	1×10^{12}	1×10^{13}
Equivalent time T_{n1} (yr)	0.12178	0.26708	2.6708	26.708
Total displacements per atom (DPA)	2.890×10^{-11}	6.647×10^{-11}	6.647×10^{-10}	6.647×10^{-9}
Equivalent time T_{n2} (yr)	0.08645	0.19883	1.9883	19.883

Table 2
Equivalent calculated values γ irradiation.

Properties	Dose point 1	Dose point 2
Dose point of Water D_γ (Gy)	309.28	927.84
Equivalent dose point of InGaAs cell (Gy)	279.90	839.69
Equivalent time T_γ (yr)	24.12	72.34

$$T_{n2}(yr) = \frac{1}{3600 \times 24 \times 365}(D_{Xd} / D_{Gd}) \quad (2)$$

where D_{Xd} is the total DPA of XPNR and D_{Gd} is the DPA per second of GPHS.

Based on the reference data (ASTM E722-14) the total DPA values of neutron spectrum were calculated (Depriest, 2019; Greenwood and Smither, 1985). The DPA calculated from the GPHS neutron spectrum is 1.06×10^{-17} dpa/s. Relevant values are shown in Table 1. Due to the variability of the XPNR and GPHS neutron spectra shown in Fig. S2(a), the total DPA value method yields an equivalent time of 19.883 years, which was more conservative compared to the cumulative total injection.

2.1.2. γ Radiation dose calculation and equivalence

The principle of total dose equivalence is usually used in evaluating γ radiation, and the equivalence of γ rays does not depend on the consistency of a γ spectrum. After comprehensive consideration of the calculation results of MCNP simulation and the data of Cheon et al. (Cheon et al., 2018; Lee et al., 2017) the dose rate of 1.325×10^{-3} Gy/h at 10 cm from the heat source center was taken as the benchmark. After considering the radiation dose rate at the Martian surface, in this work, the irradiation equivalent experiment was conducted based on a dose point of 1.334×10^{-3} Gy/h, and the equivalent service time of the InGaAs TPV cell was calculated.

The γ dose conversion factor between semiconductor and water is 0.905 (Burns, 1994; Seuntjens and Duane, 2009). The irradiation dose point of the γ acceleration equivalent experiment is $D_\gamma = 309.28$ Gy and 927.84 Gy (Water), and the corresponding InGaAs cell is 279.90 Gy and 839.69 Gy (Semiconductor). On the basis of the dose rate of the InGaAs TPV cell ($D_{r\gamma} = 1.334 \times 10^{-3}$ Gy/h), the InGaAs cell was attributed to 24.12–72.34 years of working time (calculated using Formula 3), as shown in Table 2.

$$T_\gamma(yr) = \frac{1}{24 \times 365}\left(0.905\, D_\gamma / D_{r\gamma}\right) \quad (3)$$

where D_γ is the total γ irradiation dose and $D_{r\gamma}$ is the reference γ dose calculated at InGaAs cell.

2.2. Parameters of InGaAs TPV cell

The InGaAs TPV cell is a direct bandgap semiconductor, has a high infrared energy conversion efficiency, and is a potential energy

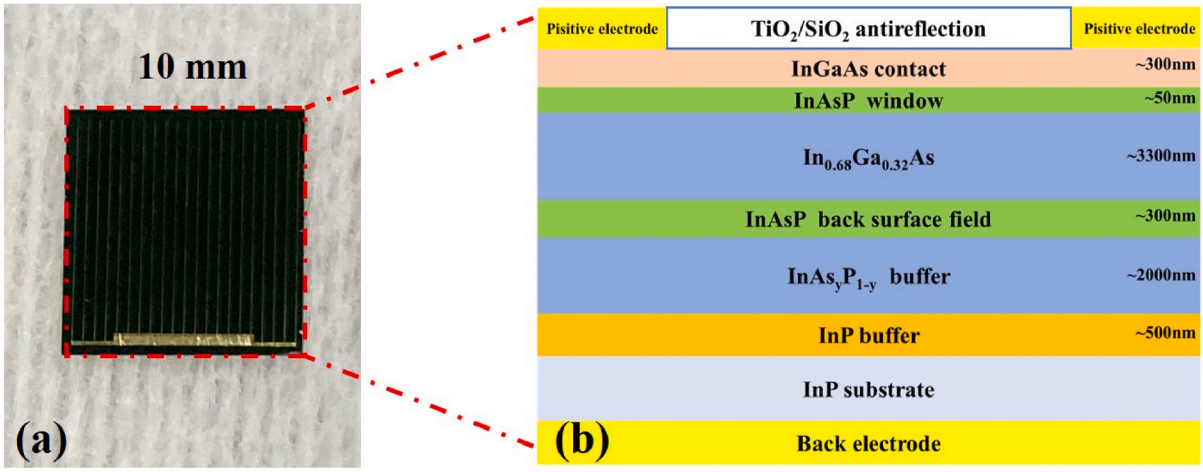

Fig. 2. (a) Prototype and (b) schematic of the side section structure of the InGaAs cell.

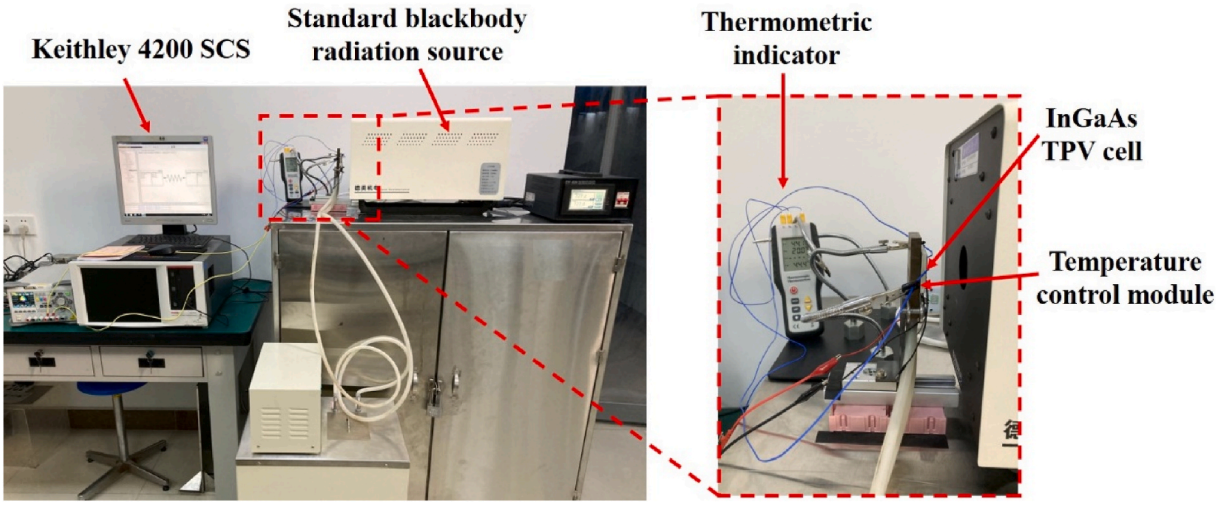

Fig. 3. InGaAs TPV Cell test platform for photoelectric characteristics and temperature effects.

conversion cell for RTPV generators. In this work, the InGaAs cell was prepared through mismatched growth and includes an InP substrate, InP buffer layer, and InGaAs functional layer, etc. as shown in Fig. 2. The InGaAs ($E_g = 0.72$ eV) TPV cell was directly fabricated on an aluminium printed circuit board (PCB) substrate with an effective area of 10 × 10 mm^2. After the links and leads were welded, follow-up irradiation and various test experiments were carried out. Before the stability test experiment, the InGaAs cells were preliminarily tested. Three identical InGaAs samples were prepared for each irradiation dose point.

2.3. QE test methods for InGaAs TPV cell

The test system of InGaAs TPV cell via the spectral response/quantum efficiency meter (Enlitech QE-R) show in Fig. S3. The InGaAs TPV cell with an effective area of 10 × 10 mm^2 was used. External quantum efficiency (EQE) and reflectance within the cell's photoelectric response range were measured by using the continuous beam and integrating sphere of the instrument. The base platform at the bottom controlled the temperature of the measured cell through a temperature control unit, and the temperature range was set at 276.5–354.5 K. The test was carried out in a dark box. The photoelectric efficiency of the InGaAs TPV cell and change in temperature before and after irradiation were evaluated using the above experimental platform. Multiple batches of InGaAs samples were tested, and the quantum efficiency results tended to be consistent within a dose group. The EQE of the InGaAs cell had a consistently high overall quantum efficiency (~80%) within a wavelength range of 500–1500 nm. After neutron irradiation, the EQE test curves of all samples in each dose group hardly fluctuated, as shown in Fig. S4.

2.4. InGaAs TPV cell photovoltaic and temperature change test conditions

Fig. 3 shows the InGaAs TPV cell model test system for determining photoelectric characteristics and temperature effects. The GPHS–RTPV system releases heat from the heat source in the form of blackbody infrared radiation, which the InGaAs cell receives and converts into electricity. The temperature of a standard blackbody radiation source (DEMEI, DY–HT3 Blackbody Furnace) is 1000 K. The temperature of the InGaAs TPV cell was determined using a temperature-measuring instrument (R7100). The InGaAs temperature was controlled through water circulation cooling and with a temperature control unit. The electrical performance of the InGaAs was tested with a parameter analyzer (Keithley 4200 SCS) in a dark environment with a normal temperature of 293.15 K and standard atmospheric pressure of 1 atm.

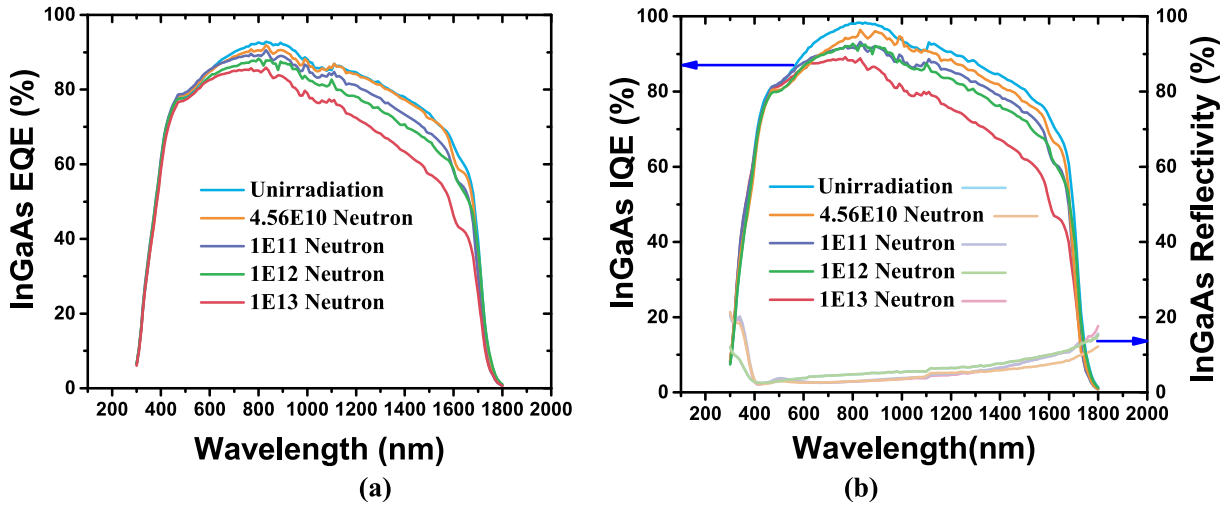

Fig. 4. (a) EQE and (b) IQE/R curves of InGaAs cells vary with neutron irradiation.

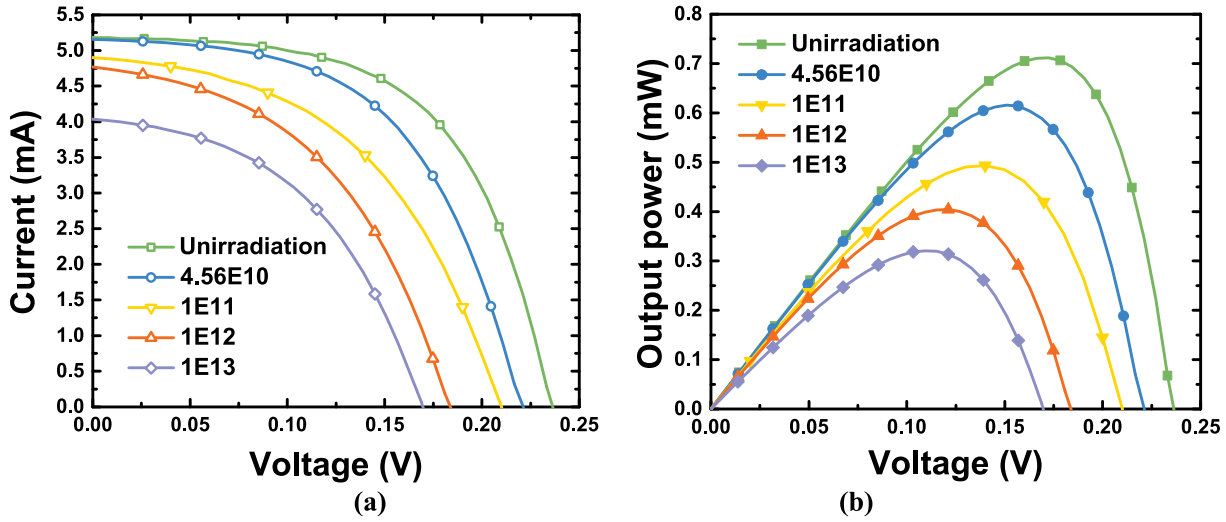

Fig. 5. (a) *I–V* and (b) *P–V* curves of the InGaAs cells at different neutron radiation doses were measured in a 1000 K blackbody spectrum.

3. Result and discussion

3.1. Analysis of the influence of neutron irradiation on InGaAs cell

3.1.1. Effect of quantum efficiency on neutron irradiation

In the neutron-irradiated InGaAs TPV cells, the EQE test data of different samples in the same dose group were integrated for the drawing of comparison curves at different dose points, as shown in Fig. 4 (a). After different doses of neutron irradiation, the EQE of the InGaAs cell decreased at varying degrees. At the equivalent of serving dose of neutrons at 1×10^{13} n/cm^2, the overall EQE of the InGaAs cells was attenuated by 11.65% compared with that of the unirradiated samples. Notably, the attenuation rate was 19.90% in the spectral band (1100–1800 nm) used in the RTPV system. The internal quantum efficiency (IQE) obtained after the influence of surface reflectivity was reduced reflected the photoelectric response inside the cell. The IQE was calculated using Formula (4), as shown in Fig. 4(b). The surface reflectance of InGaAs cells were not affected by variations in the level of neutron injection. The attenuation trend of the IQE curves of the InGaAs after neutron irradiation was basically the same as that of EQE curves.

$$IQE = EQE / (1 - R) \tag{4}$$

As mentioned above, neutron irradiation had a more serious impact on photoelectric conversion in the 1100–1800 nm band of the InGaAs cell and a weaker impact on the 300–1100 nm spectral band. The possible reason was that neutron irradiation damaged the gap holes in the InGaAs cell PN junction, and the transition holes with low-energy levels were more vulnerable to radiation damage. Therefore, the number of low energy photon transition excitations was reduced. Meanwhile, hole structure damage increased photoelectron recombination, further reducing the efficiency of photoelectron collection in the photovoltaic effect.

3.1.2. Electrical properties chang with neutron irradiation in blackbody infrared spectrum

The electrical output characteristics of InGaAs cells in the actual working blackbody spectrum were further evaluated. Fig. 5(a) shows the current–voltage (*I–V*) characteristic curves on an InGaAs TPV cell in 1000 K blackbody spectra. The output power–voltage (*P–V*) curves were obtained on the basis of the *I–V* curves and Equation (5), as shown in Fig. 5(b). The *I–V* and *P–V* curves of the InGaAs at different neutron irradiation doses were measured. As the neutron irradiation dose increased, the *I–V* and *P–V* curves presented specific change laws. The potential reason was that neutron irradiation caused damage to the PN junction regions of the InGaAs cells, and resulting defects affected the generation of recombination and drift of carriers. The effects caused

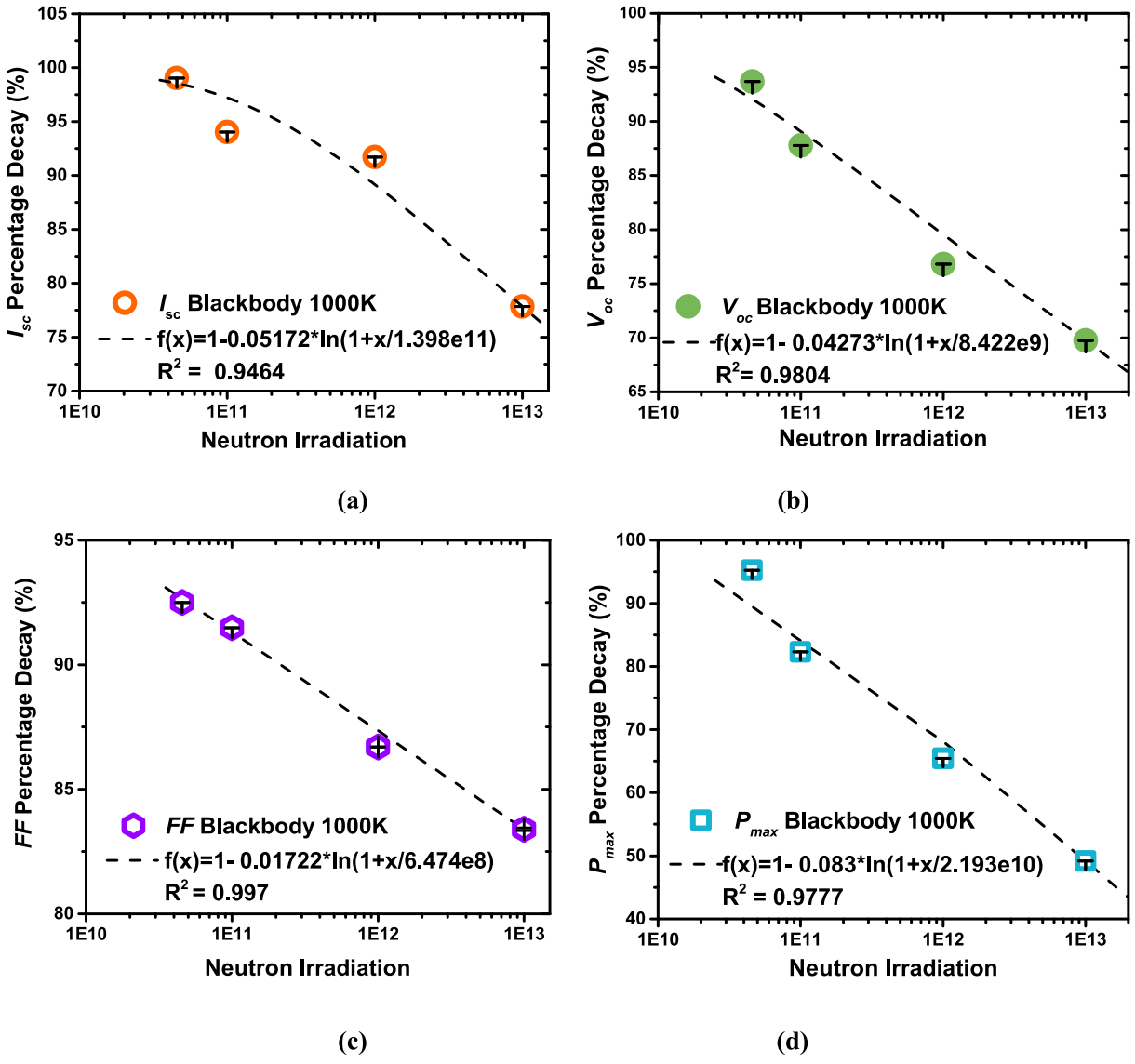

Fig. 6. (a) I_{sc}, (b) V_{oc}, (c) *FF*, and (d) P_{max} of the InGaAs cells at varied neutron irradiation doses.

macroscopic changes in current and voltage parameters.

$$P = I \times V \tag{5}$$

The electrical parameters of the InGaAs cell, including I_{sc}, V_{oc}, maximum output power (P_{max}), and fill factor (*FF*) were extracted. The calculation relationship between each parameter follows Formula (6).

$$P_{max} = FF(V_{oc} \cdot I_{sc}) \tag{6}$$

The irradiation degradation on electrical parameters (I_{sc}, V_{oc}, *FF*, and P_{max}) can be predicted by the following semi-empirical expression of Formula (7)(Anspaugh, 1996; Warner et al., 2003).

$$Y = 1 - C\ln(1 + D_r / D) \tag{7}$$

where Y represents the attenuation percentage of I_{sc}, V_{oc}, *FF*, or P_{max}; D_r represents the irradiation dose of the InGaAs cells; and C and D are the fitting parameters. The variation trend of electrical parameters of extracted InGaAs cells with neutron irradiation is shown in Fig. 6.

All the electrical output performance parameters of RTPV showed a decay trend with increasing irradiation dose, and the curves fitted by Formula(6) were basically consistent with the experimental results. At 1 $\times$ 10^{13} neutron irradiation dose, I_{sc} decreased by about 78% of its initial value, the V_{oc} decreased to 70% of the initial value. After synthesis of the

Table 3
Fitting parameters of Formula 6 to I_{sc}, V_{oc}, *FF*, and P_{max} degradation curves.

Parameters	C	D	R^2
I_{sc}	0.05172	1.398E11	0.9464
V_{oc}	0.04273	8.422E9	0.9804
FF	0.01722	6.474E8	0.9970
P_{max}	0.08302	2.193E10	0.9777

V_{oc}, I_{sc}, and *FF* parameters (Formula 5), P_{max} decreased with neutron irradiation. Under neutron irradiation of 1 $\times$ 10^{13} n/cm^2, the P_{max} of the InGaAs cell decreased to 50.15% of the initial value. Meanwhile, C, D and coefficient of determination R^2 obtained by fitting each electrical parameter are shown in Table 3.

3.2. Analysis of the influence of γ irradiation on InGaAs cell

3.2.1. Effect of quantum efficiency on γ irradiation

EQE and IQE/R curves obtained after γ irradiation at two dose points (309.28 and 927.84 Gy) are shown in Fig. 7. The EQE, IQE and reflectivity of the cells was almost unchanged under the irradiation at two different deposition doses of γ photons compared with that in the

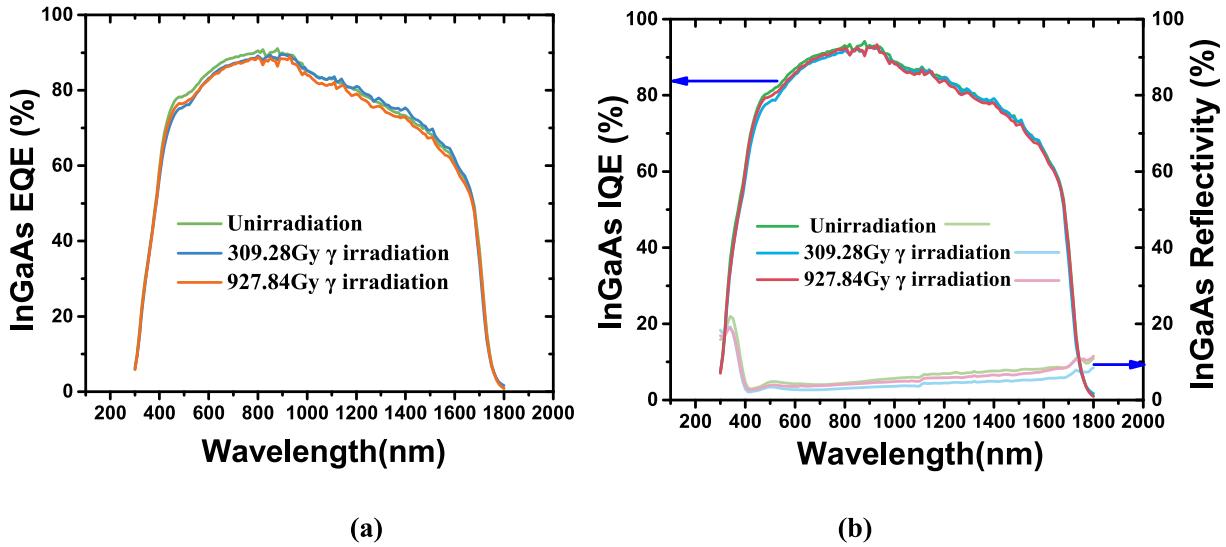

Fig. 7. (a) EQE and (b) IQE/R curves of InGaAs cells vary with γ irradiation.

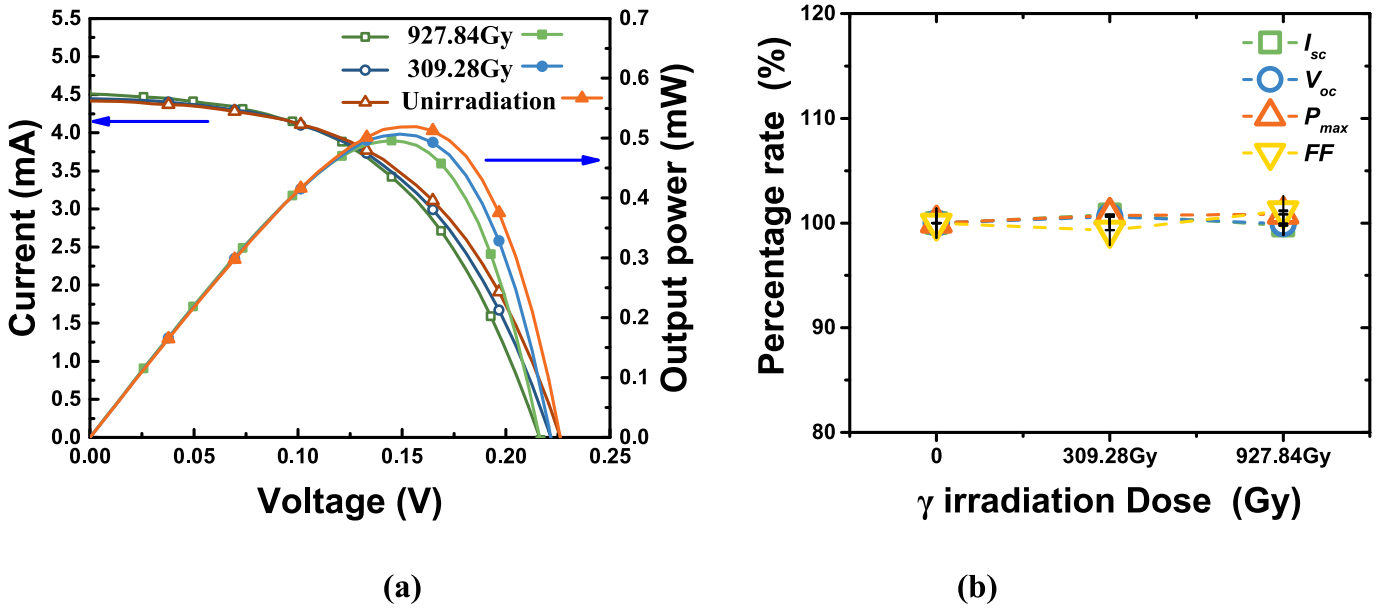

Fig. 8. (a) *I–V/P–V* curves and (b) electrical parameters of InGaAs cells at different γ radiation doses were measured in the 1000 K blackbody spectrum.

unirradiated. This result indicated that in the GPHS–RTPV system, the attenuation of EQE, IQE, and reflectivity in InGaAs cells was almost negligible after about 72.34 years of γ ray irradiation.

3.2.2. Electrical properties changes with γ irradiation in the blackbody infrared spectrum

InGaAs cells were irradiated with two different total doses of γ rays, and their electrical performance were tested under the infrared radiation of the 1000 K blackbody. The *I–V/P–V* curves of the two different γ dose points were basically consistent with those of the unirradiated samples, and the electrical output parameters P_{max}, V_{oc}, I_{sc}, and *FF* did not change significantly after γ irradiation, as shown in Fig. 8. Compared with neutron irradiation, γ irradiation caused little damage to the InGaAs TPV cells.

3.3. Analysis of neutron and γ co-irradiation effect and service life of GPHS–RTPV

In the GPHS–RTPV system, given the actual service situation of the InGaAs cell, the effects of neutron and γ irradiation were discussed in combination. The InGaAs cells irradiated by a 1×10^{13} n/cm^2 reactor neutron source was selected for subsequent 927.84 Gy Co–60 γ source radiation. After successive neutron and γ irradiation, the EQE/IQE curves of the cells showed no significant change compared with those of the cells irradiated by neutron alone, as shown in Fig. 9 (a) and (b).

The photoelectric test under 1000 K standard blackbody radiation source showed that the InGaAs cell, which had been seriously damaged after 1×10^{13} n/cm^2 neutron dose irradiation, was still unaffected after 927.84 Gy of γ irradiation, as shown in Fig. 9 (c) and (d). In the accelerated neutron/γ irradiation, the effect of γ ray irradiation on GPHS–RTPV was almost negligible, whereas the effect of neutron irradiation on the InGaAs cell was extremely significant. The reason was that the high-energy γ rays had strong penetration and easily passed

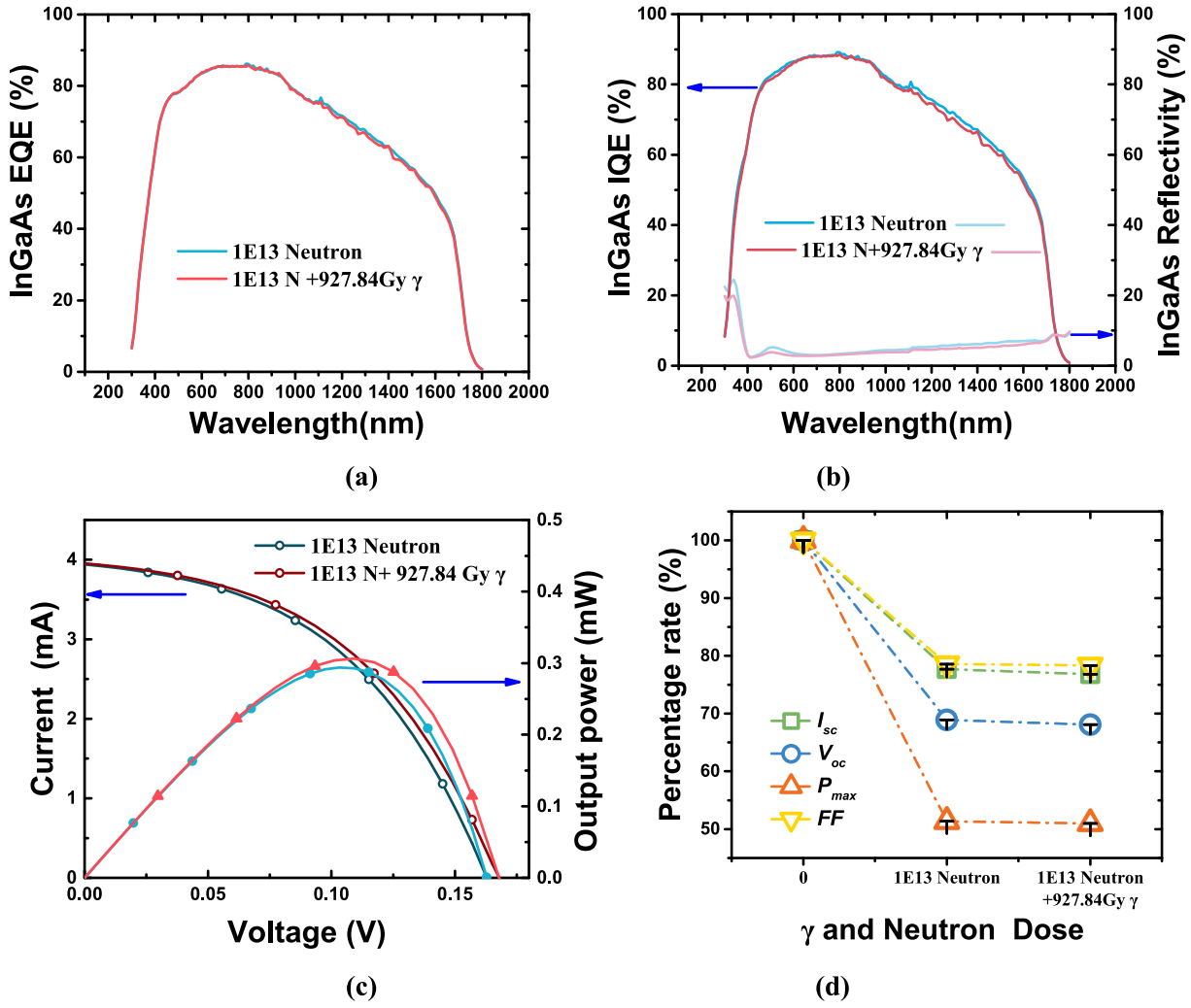

Fig. 9. (a) EQE and (b) IQE/R curves of InGaAs cells at neutron irradiation followed by γ irradiation. (c) *I–V/P–V* curves of InGaAs cells at neutron irradiation followed by γ irradiation, which were measured in a 1000 K blackbody spectrum. (d) The correspondingly I_{sc}, V_{oc}, *FF*, and P_{max} of the InGaAs cells varied with neutron and γ irradiation doses.

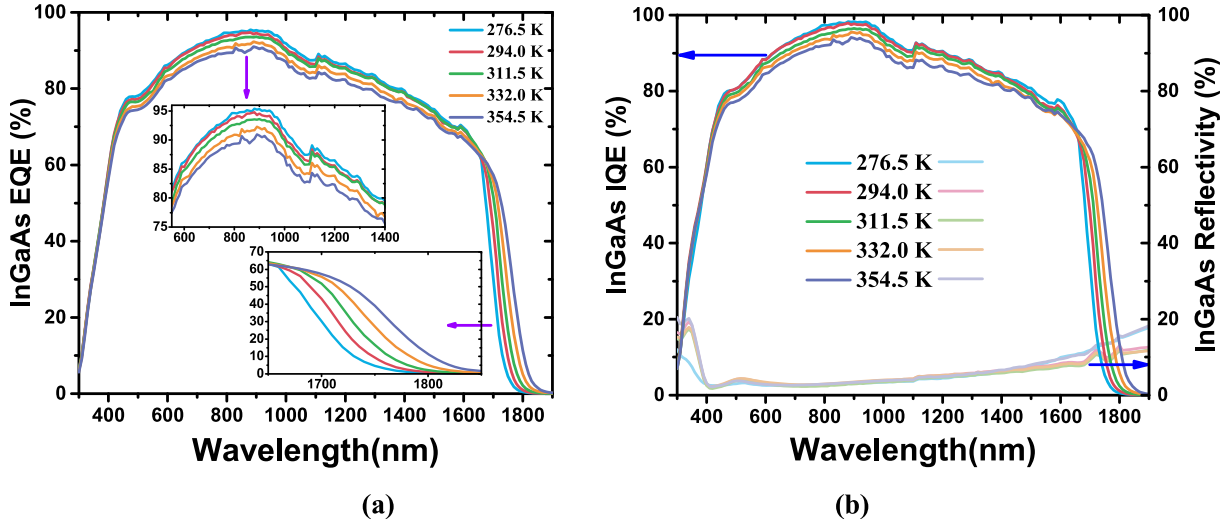

Fig. 10. (a)EQE and (b)IQE/R curves of InGaAs cell at different temperatures.

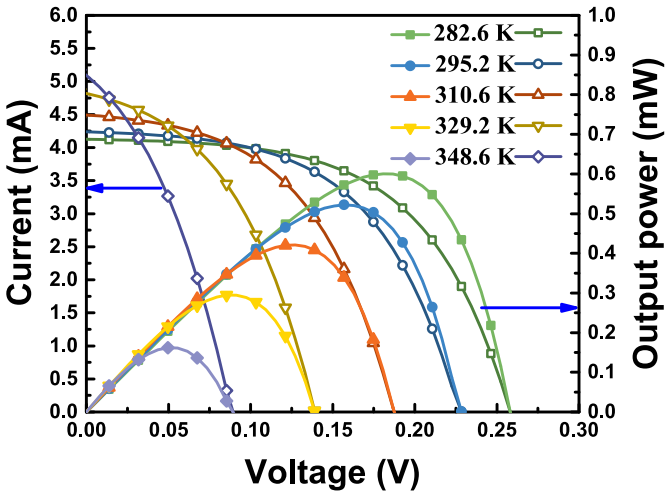

Fig. 11. *I–V/P–V* curves of InGaAs cells at different temperatures were measured in a 1000 K blackbody spectrum.

through the InGaAs cell, inhibiting energy deposition and causing minor effects. In addition, compared with neutrons, γ rays with the same energy had a lower radiation weight factor and weaker damaging effects on the InGaAs cell.

3.4. Temperature stability analysis of the InGaAs cell

During the operation of GPHS–RTPV, InGaAs cell was irradiated not only by neutron and γ from a radioisotope heat source but also by heat flux from high temperature heat source. Given that the GPHS–RTPV operates in the complex temperature environment of space, the temperature of the InGaAs cell is usually in a state of constant change. Therefore, analyzing change in a cell at different temperatures through experiments is extremely important. The temperature range selected (270–360 K) is the normal operating range of TPV cells and ensures that InGaAs cells operate properly and are not damaged.

3.4.1. Quantum efficiency of InGaAs changes with temperature

The EQE and IQE curves of the InGaAs cell at different temperatures were measured, as shown in Fig. 10. As the InGaAs cell temperature increased, the EQE/IQE curves were broadened to longer wavelengths, but the overall values were reduced. And the reflectivity of the InGaAs

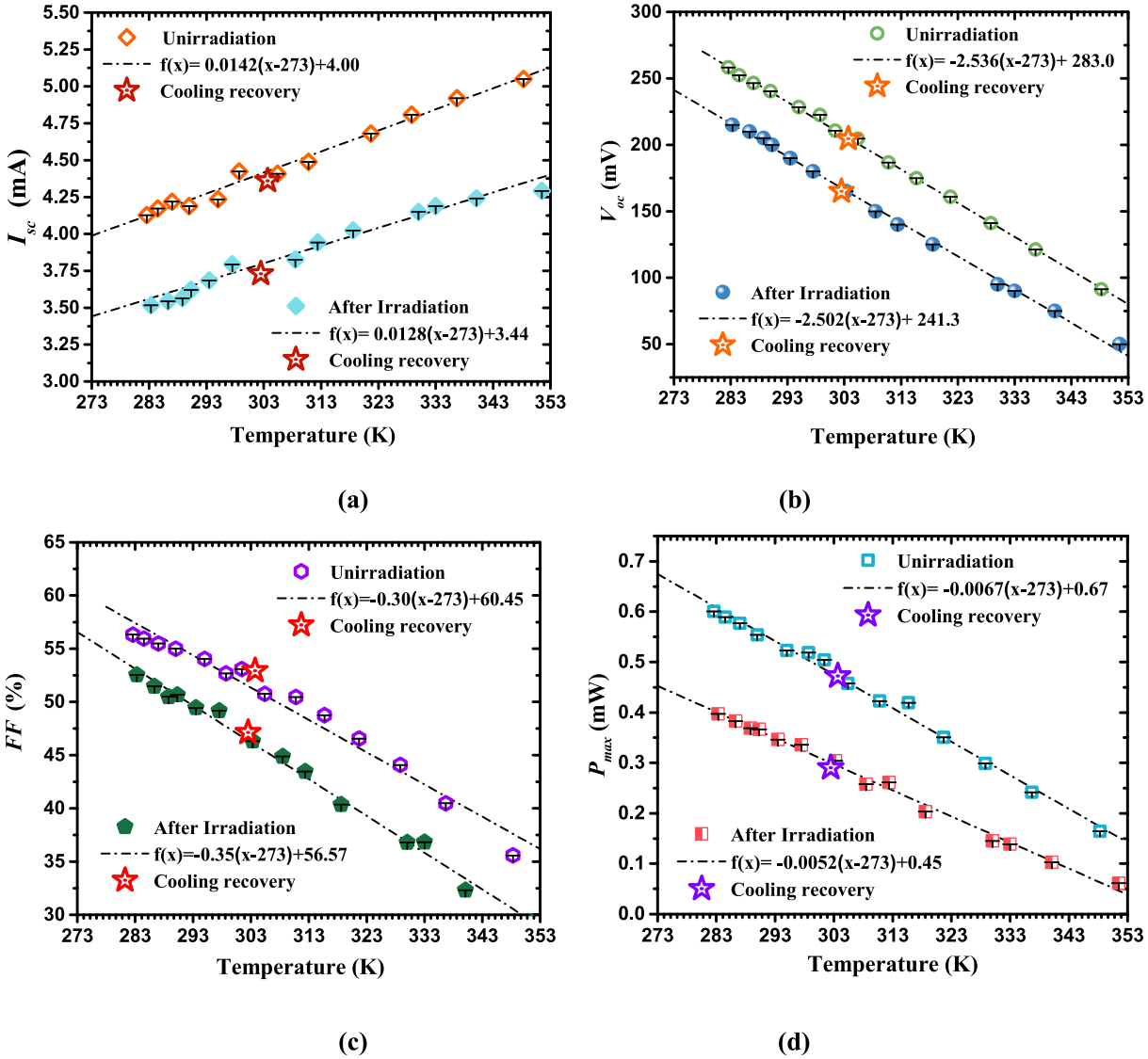

Fig. 12. The (a) I_{sc}, (b) V_{oc}, (c) *FF*, and (d) P_{max} of InGaAs cell varied with temperature.

Table 4
Electrical parameters of InGaAs cell with temperature change rate.

Gradient	I_{sc} (μA/K·cm^2)	V_{oc} (mV/K)	*FF* (%/K)	P_{max} (μW/K·cm^2)
before irradiation	14.2	−2.536	−0.3	−6.7
after irradiation	12.8	−2.502	−0.35	−5.2

cell was not affected with the change of temperature. As the temperature (T_c) increased from 276.5 K to 354.5 K, the EQE/IQE curves were numerically attenuated by 4.874% in the 500–1600 nm band and expanded by 80 nm in the 1600–1900 nm. The decay of the EQE/IQE values reduced the photoelectric conversion efficiency, whereas the expansion of the curve indicated that the InGaAs cell responds to wider spectrum of incident spectrum, with more infrared photons being included. Therefore, for the systematic analysis of the influence of temperature on the photovoltaic output of InGaAs cell, further analysis of the electrical properties is required.

3.4.2. Electrical properties changes with temperature in the blackbody infrared spectrum

Under the 1000 K blackbody radiation spectrum, the *I–V/P–V* curves of the InGaAs cell changed with temperature (Fig. 11). The linear trend of I_{sc}, V_{oc}, P_{max}, and *FF* at varied temperatures shows in Fig. 12. In addition, the temperature change of the cell after neutron and γ irradiation was also tested to explore the effect of InGaAs cells on temperature change after irradiation. As the cell temperature changed from 282.6 K to 348.6 K, I_{sc} increases with temperature, while V_{oc} and P_{max} decrease with increasing temperature, and the trend with temperature is shown in Table 4. The gradients of the above electrical parameters at varied temperatures were almost the same before and after irradiation, so irradiation had almost no influence on the sensitivity of the InGaAs cells to temperature change.

When the temperature of InGaAs cell was naturally cooled from 348.6 K to 300 K, electrical parameters, such as P_{max}, V_{oc}, I_{sc}, and *FF* were restored to their original values (Star point in Fig. 12). Therefore, the degradation of InGaAs cell performance at a high temperature within the experimental range was reversible and did not cause harm to the cell itself.

In general, the output power of InGaAs cell increased with decreasing temperature. When the temperature increased beyond ~373 K, the P_{max} was close to zero. After irradiation, the sensitivity of the InGaAs cell to temperature did not increase significantly, and the change rate of P_{max} decreased to a certain extent. Therefore, for the operation of GPHS–RTPV, it is necessary to ensure a lower ambient temperature, so as to give full play to its better application potential. To deal with the alternating environment of large temperature differences, consider adjusting the GPHS–RTPV by using power management to maintain smooth power output.

It's worth noting that during this entire research cycle, the InGaAs cell has been sitting at room temperature for more than 300 days. After the above data were obtained by neutron and γ irradiation and temperature experiment, InGaAs cells were sampled from each group and the experiment was repeated. The QE/*I–V* data of InGaAs cell measured at 1 day intervals showed no fluctuation compared with 300 days ago, as shown in Fig. 13. The performance of the InGaAs cell itself and its degradation characteristics under irradiation did not change with time at room temperature. This result showed that the cell has good storage stability. The output performance of the GPHS–RTPV did not deteriorate over time in a stable environment for a certain period of time. The InGaAs cell will also not be irreversibly damaged by temperature change. Thus, the neutron and γ radiation generated by GPHS is an important factor affecting the lifetime of RTPV.

In summary, the photon irradiation and long-term operation have a minimal impact on the performance degradation of InGaAs cells. Furthermore, the effects of temperature variations on InGaAs cells were reversible. And the performance degradation observed in InGaAs cells during service primarily stems from neutron irradiation. Therefore,the main factor affecting the service life of the GPHS-RTPV system is the performance degradation of the InGaAs cell due to neutron irradiation damage. The results of the irradiation experiments show that after 19.883 years of equivalent GPHS–RTPV service, the P_{max} of the InGaAs cell was maintained at 50.15% of the initial value, and then the service life of the GPHS–RTPV with InGaAs cell can be presumed to be at least 19.883 years. Its operating life is expected to further improve when a neutron shield is installed inside the GPHS. Notably, the half-life of the radioisotope itself is not considered in the assessed of service time. Over time, the intensity of neutron and γ radiation from radioisotope decay gradually decreases. Therefore, the life evaluation in this work is relatively conservative, and the actual equivalent life may be more optimistic than this result.

4. Conclusions

A 500 W GPHS was used as a benchmark for the analysis of the service lives and stability of GPHS–RTPV generators under real working conditions. In this work, InGaAs TPV cells were subjected to neutron and γ radiation from the equivalent GPHS. Given the heat of GPHS and

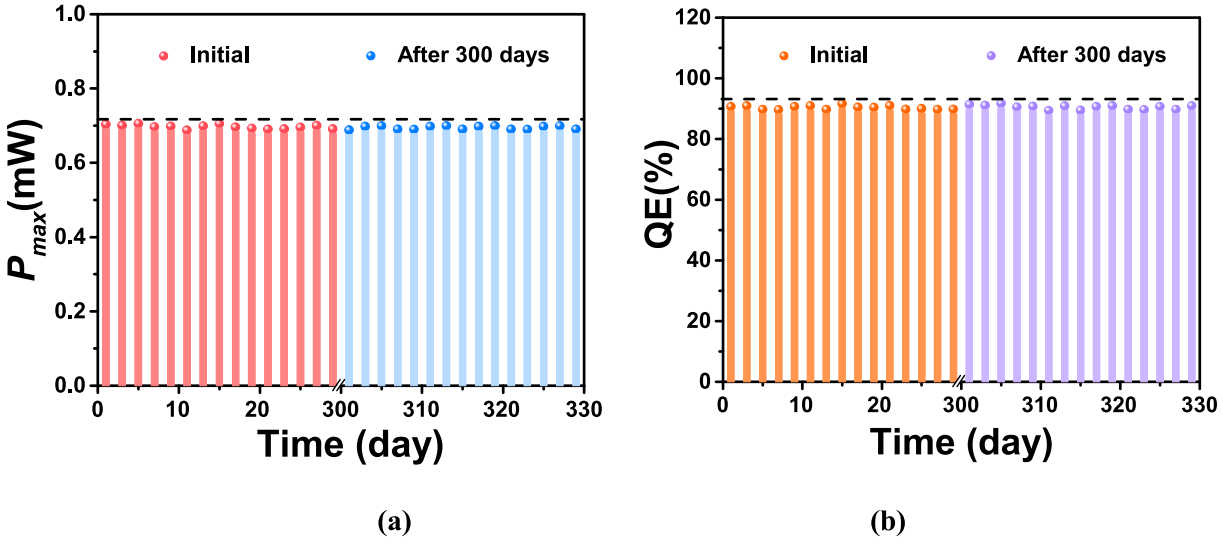

Fig. 13. (a) P_{max} and (b) maximum QE of InGaAs cell were compared at the initial and after 300 days.

complex temperature of the InGaAs cells in the space environment, the effect of temperature on its performance was discussed through experiments. The effects of neutron and γ irradiation and temperature on the InGaAs cells were analyzed using EQE/IQE and electrical output measurements. The InGaAs cells exhibited varying degrees of damage and degradation under neutron irradiation, whereas γ radiation almost had no effect. After the accumulated neutron and γ irradiation, the initial power can still be maintained at 50.15%. The performance of InGaAs cells varies linearly with cell temperature. The output power increases by 6.7 μW/cm^2 for every 1 K decrease in temperature over the range of 270–360 K. When the temperature returns from high temperature to room temperature, the output of the cell still returns to the original value. The performance of GPHS–RTPV generators will be higher in a stable low-temperature space environment, and their service lives are conservatively estimated at 19.883 years. The life of GPHS–RTPV can be effectively extended by adding a radiation shield (mainly neutrons) inside the GPHS. This study provides insights into the InGaAs TPV cell's influence on irradiation and temperature changes under actual working conditions, providing a reference for life prediction and stability evaluation of GPHS–RTPV generators.

Declaration of competing interest

The authors declare that they have no known competing financial interests or personal relationships that could have appeared to influence the work reported in this paper.

Data availability

The authors do not have permission to share data.

Acknowledgements

This work is supported by the National Natural Science Foundation of China (Grant Nos. 12275132 and 12075119), China Postdoctoral Science Foundation (Grant No. 2022M711613), the Postgraduate Research & Practice Innovation Program of Jiangsu Province (Grant No. KYCX21_0205), and the Shanghai Aerospace Science and Technology Innovation Foundation (Grant No. SAST 2020-097).

Appendix A. Supplementary data

Supplementary data to this article can be found online at https://doi.org/10.1016/j.pnucene.2023.104807.

References

Anspaugh, B.E., 1996. GaAs solar cell radiation handbook. Jet Propulsion Laboratory, 96-9 5-5-5–7.

Barklay, C.D., Kramer, D.P., Ruhkamp, J.D., 2005. Analysis of the effect of time, temperature, and fuel age on helium release from 238-plutonium dioxide fuel. AIP Conf. Proc. 746, 820–826. https://doi.org/10.1063/1.1867203.

Barklay, C.D., Kramer, D.P., Talnagi, J., 2007. Investigation of effects of neutron irradiation on tantalum alloys for radioisotope power system applications. AIP Conf. Proc. 880, 224–228. https://doi.org/10.1063/1.2437459.

Blandre, E., Vaillon, R., Drévillon, J., 2019. New insights into the thermal behavior and management of thermophotovoltaic systems. Opt Express 27, 36340. https://doi.org/10.1364/oe.27.036340.

Burns, J.E., 1994. Absorbed-dose calibrations in high-energy photon beams at the National Physical Laboratory: conversion procedure. Phys. Med. Biol. 39, 1555–1575. https://doi.org/10.1088/0031-9155/39/10/004.

Cheon, S.J., Hong, S.G., Lee, J.H., Nam, Y.S., 2018. Design and performance analysis of a 500-W heat source for radioisotope thermophotovoltaic converters. Int. J. Energy Res. 42, 817–829.

Chubb, D., 2007. Fundamentals of Thermophotovoltaic Energy Conversion (Google eBook). Elsevier.

Crowley, C.J., Elkouh, N.A., Murray, S., Chubb, D.L., 2005. Thermophotovoltaic converter performance for radioisotope power systems. AIP Conf. Proc. 746, 601–614. https://doi.org/10.1063/1.1867178.

Datas, A., Martí, A., 2017. Thermophotovoltaic energy in space applications: review and future potential. Sol. Energy Mater. Sol. Cells 161, 285–296. https://doi.org/10.1016/j.solmat.2016.12.007.

Depriest, K.R., 2019. Historical Examination of the ASTM Standard E722 1-MeV Silicon Equivalent Fluence Metric. Sandia National Laboratories (SNL), Albuquerque, NM, and Livermore, CA.

Greenwood, L.R., Smither, R.K., 1985. SPECTER: Neutron Damage Calculations for Materials Irradiations. Argonne National Lab., IL (USA).

Hongliang, G., Linfeng, S., Qiang, S., Qiming, Z., Yiyong, W., Jingdong, X., Bin, G., Yanqing, Z., 2019. Degradation of up-grown metamorphic InGaP/InGaAs/Ge solar cells by low-energy proton irradiation. Sol. Energy Mater. Sol. Cells 191, 399–405. https://doi.org/10.1016/j.solmat.2018.11.033.

Koudelka, R.D., Murray, C.S., Fleming, J.G., Shaw, M.J., Teofilo, V., Alexander, C., 2006. Radioisotope micropower system using thermophotovoltaic energy conversion. AIP Conf. Proc. 813, 545–551. https://doi.org/10.1063/1.2169233.

Lee, J., Cheon, S., Hong, S., Nam, Y., 2017. A radioisotope thermophotovoltaic converter with nanophotonic emitters and filters. Int. J. Heat Mass Tran. 108, 1115–1125. https://doi.org/10.1016/j.ijheatmasstransfer.2016.12.049.

Liu, Junjun, 2003. An assessment of the global, seasonal, and interannual spacecraft record of Martian climate in the thermal infrared. J. Geophys. Res. Planets 108, 5089.

Liu, K., Tang, X., Liu, Y., Xu, Z., Yuan, Z., Ji, D., Ramakrishna, S., 2020a. Experimental optimization of small–scale structure–adjustable radioisotope thermoelectric generators. Appl. Energy 280, 115907. https://doi.org/10.1016/j.apenergy.2020.115907.

Liu, K., Tang, X., Liu, Y., Xu, Z., Yuan, Z., Zhang, Z., 2020b. Enhancing the performance of fully-scaled structure-adjustable 3D thermoelectric devices based on cold–press sintering and molding. Energy 206, 118096. https://doi.org/10.1016/j.energy.2020.118096.

Long, J., Xiao, M., Huang, X., Xing, Z., Li, X., Dai, P., Tan, M., Wu, Y., Song, M., Lu, S., 2019. High efficiency thin film GaInP/GaAs/InGaAs inverted metamorphic (IMM) solar cells based on electroplating process. J. Cryst. Growth 513, 38–42. https://doi.org/10.1016/j.jcrysgro.2019.02.057.

Martín, D., Algora, C., 2004. Temperature-dependent GaSb material parameters for reliable thermophotovoltaic cell modelling. Semicond. Sci. Technol. 19, 1040–1052. https://doi.org/10.1088/0268-1242/19/8/015.

Rinehart, G.H., 2001. Design characteristics and fabrication of radioisotope heat sources for space missions. Prog. Nucl. Energy 39, 305–319.

Schock, A., Mukunda, M., Or, C., Kumar, V., Summers, G., 1995. Design, analysis, and optimization of a radioisotope thermophotovoltaic (RTPV) generator, and its applicability to an illustrative space mission. Acta Astronaut. 37, 21–57.

Schock, A., Or, C.T., Kumar, V., 1996. Modified design of radioisotope thermophotovoltaic generator to mitigate adverse effect of measured cell voltage. Proc. Intersoc. Energy Convers. Eng. Conf. 2, 979–986. https://doi.org/10.1109/iecec.1996.553832.

Seuntjens, J., Duane, S., 2009. Photon absorbed dose standards. Metrologia 46. https://doi.org/10.1088/0026-1394/46/2/S04.

Strauch, J., Klein, A., Charles, P., Murray, C., Du, M., 2015. Radioisotope fueled thermophotovoltaic power systems for space applications. Nucl. Emerg. Technol. Space, NETS 2015 366–375.

Vining, C.B., Bennett, G.L., 2010. Power for science and exploration: upgrading the general-purpose heat source radioisotope thermoelectric generator (GPHS-RTG). 8th Annu. Int. Energy Convers. Eng. Conf. https://doi.org/10.2514/6.2010-6598.

Wang, H., Tang, X., Liu, Y., Xu, Z., Yuan, Z., Liu, K., Zhang, Z., Jiang, T., 2020. Thermal emission-enhanced and optically modulated radioisotope thermophotovoltaic generators. Energy Technol. 8 https://doi.org/10.1002/ente.201901170.

Wang, H., Xu, Z., Yuan, Z., Liu, K., Meng, C., Tang, X., 2022. High-temperature and radiation-resistant spinel-type ferrite coating for thermo-optical conversion in radioisotope thermophotovoltaic generators. Energy 239, 122255. https://doi.org/10.1016/j.energy.2021.122255.

Wang, X., Liang, R., Fisher, P., Chan, W., Xu, J., 2020a. Radioisotope thermophotovoltaic generator design methods and performance estimates for space missions. J. Propul. Power 36, 593–603. https://doi.org/10.2514/1.B37623.

Wang, X., Liang, R., Fisher, P., Chan, W., Xu, J., 2020b. Critical design features of thermal-based radioisotope generators: a review of the power solution for polar regions and space. Renew. Sustain. Energy Rev. 119, 109572 https://doi.org/10.1016/j.rser.2019.109572.

Warner, J.H., Walters, R.J., Messenger, S.R., Summers, G.P., Khanna, S.M., Estan, D., Erhardt, L.S., Houdayer, A., 2003. High Energy Proton Irradiation Effects in GaAs Devices. Eur. Sp. Agency, (Special Publ. ESA SP 2003-Septe, 525–531.

Wolford, D.S., Chubb, D.L., 2009. Theoretical performance of a radioisotope thermophotovoltaic (RTPV) power system. In: 7th International Energy Conversion Engineering Conference, p. 4655. https://doi.org/10.2514/6.2009-4655.

Yuan, Z., Tang, X., Xu, Z., Li, J., Chen, W., Liu, K., Liu, Y., Zhang, Z., 2018. Screen-printed radial structure micro radioisotope thermoelectric generator. Appl. Energy 225, 746–754.

Zeitlin, C., Cleghorn, T., Cucinotta, F., Saganti, P., Andersen, V., Lee, K., Pinsky, L., Atwell, W., Turner, R., Badhwar, G., 2004. Overview of the Martian radiation environment experiment. Adv. Space Res. 33, 2204–2210. https://doi.org/10.1016/S0273-1177(03)00514-3.